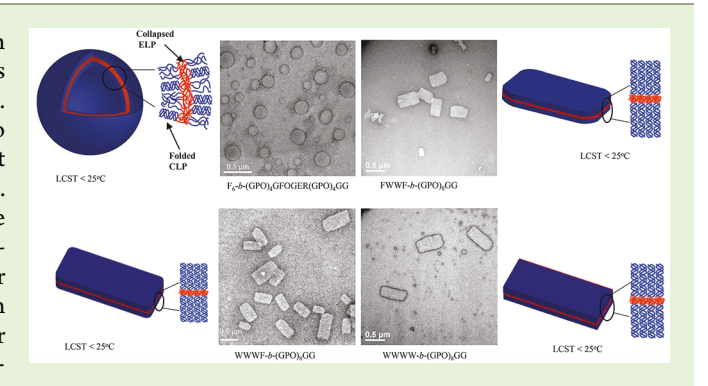


Self-Assembly of Stable Nanoscale Platelets from Designed Elastinlike Peptide-Collagen-like Peptide Bioconjugates

Jingya Qin,[†] Tianzhi Luo,[†] and Kristi L. Kiick*,^{†,‡}

Supporting Information

ABSTRACT: The self-assembly of nanostructures from elastin-like (poly)peptide (ELP) containing block copolymers has been a subject of intense investigation over decades. However, short synthetic ELPs have rarely been used due to their high inverse transition temperature; the use of short ELPs has largely been limited to polymer conjugates. Motivated by our previous work which successfully overcame this barrier by simply conjugating short ELPs with a triplehelix-forming collagen-like peptide, in this study, we further extend the ELP library to a series of ELPs equipped with aromatic residues and having sequences as short as four pentapeptide motifs. The resulting elastin-like peptidecollagen-like peptide (ELP-CLP) bioconjugates unexpectedly



self-assembled into nanosized platelets likely by forming a bilayer structure. Given the previously demonstrated ability of many other CLP conjugates to target collagens and the potential for encapsulation of hydrophobic drugs in collapsed ELPs, these ELP-CLP nanoplatelets may offer similar opportunities for targeted delivery in biomedical and other arenas.

INTRODUCTION

Peptide-based bioconjugates have been intensely explored over multiple decades as building blocks for self-assembled nanostructures with applications as smart drug delivery vehicles and tissue engineering substrates. Short synthetic collagen-like peptides (CLPs), also known as collagen-mimetic peptides (CMPs), with the ability to mimic the triple-helix conformation of native collagen, have been widely used to study the stabilization effect of specific peptide sequences in collagen triple helices^{4–9} as well as to mimic collagen fibril formation. Additionally, more recent studies have demonstrated that unfolded CLPs are capable of targeting native collagens and collagen substrates via the formation of a triple helix. ^{14–26} In spite of these wide applications, the use of CLPs as building blocks for the fabrication of nanostructures for drug delivery has been rarely reported. 1,27-30

Elastin-like (poly)peptides are artificial biopolymers composed of the pentapeptide repeat Val-Pro-Gly-Xaa-Gly.³¹ Similar to the behavior of thermoresponsive synthetic polymers, a characteristic property of ELPs is their lower critical solution temperature (LCST)-like behavior (also termed an inverse transition temperature),32 which endows ELPs with the ability to be used as building blocks for the assembly of nanostructures.^{33–37} A wide variety of studies have demonstrated the versatility of ELP design and resulting transition temperature and the application of these principles to the production of hydrogel matrices and drug delivery vehicles. 40-44 While these studies illustrate the

versatility of the ELPs as self-assembling building blocks, essentially all of the ELPs employed are recombinamers with tens or even hundreds of pentapeptide repeats. Short synthetic ELPs (peptides) on their own have been rarely used as bulk materials for biomedical applications, possibly due to their relatively high transition temperature, 38,39 although recent studies suggest the utility of the conjugation of short ELPs to polymers and dendrimers to control LCST-like behavior and self-assembly⁴⁵⁻⁴⁹ as well as the impact of protecting groups on the thermally induced transitions of short ELPs.⁵

In our previous work, we demonstrated that this limitation can be easily overcome by simply conjugating short ELPs with a triple-helix-forming CLP. 51 The resulting ELP-CLP bioconjugate exhibited a remarkable reduction in the inverse transition temperature (T_t) of the ELP domain upon formation of the CLP triple helix, so that nanostructures can be formed under aqueous conditions in a temperature range of relevance for biomaterials applications. The lower transition temperature of the conjugate enabled the facile formation of well-defined vesicles at physiological temperature and the unexpected resolubilization of the vesicles at elevated temperatures upon unfolding of the CLP domain.⁵¹ Because these vesicles exhibit thermoresponsiveness that can be used to trigger the release of cargo, the ability to bind collagen, and excellent cytocompat-

Received: November 21, 2018 Revised: February 11, 2019 Published: February 21, 2019

1514

Department of Materials Science and Engineering, University of Delaware, Newark, Delaware 19716, United States

[‡]Delaware Biotechnology Institute, Newark, Delaware 19711, United States

ibility,²⁶ they offer significant opportunities for the delivery of drugs to collagen-containing matrices and tissues.

In this report, we further investigated the inverse transition behavior and morphology of additional ELP-CLP conjugates by tuning the length and hydrophobicity of the ELP domain. ELP domains comprising (VPGXG)4, in which the number of repeats equipped with F or W residues in the X position was varied, were produced and were conjugated to the collagen-like peptide domain (GPO)₈GG. The successful production of the peptides and conjugates was verified by chromatographic methods, electrospray ionization mass spectrometry (ESI-MS), ¹H nuclear magnetic resonance spectrometry (¹H NMR), and Fourier transform infrared spectroscopy (FTIR). The conformational and assembly properties of the peptides and conjugates were characterized via circular dichroism spectroscopy (CD), dynamic light scattering (DLS), transmission electron microscopy (TEM), and atomic force microscopy (AFM). In contrast to our previously reported vesicle structures for this class of bioconjugates, nanoscale platelet morphologies resulted from the assembly process, underpinning the sensitivity of the assembly of these molecules on the amino acid composition of the elastin-like peptide domain.

EXPERIMENTAL METHODS

Materials. Fmoc-protected amino acids including Fmoc-propargylglycine, *N,N,N',N'*-tetramethyl-*O*-(1*H*-benzotriazol-1-yl)-uronium hexafluorophosphate (HBTU), and piperidine for solid-phase peptide synthesis were purchased from AAPPTEC Inc. (Louisville, KY). Rink amide polystyrene resin for solid-phase peptide synthesis was purchased from CEM Corporation (Matthews, NC). HPLC-grade acetonitrile, dimethylformamide (DMF), and copper wire were purchased from Fisher Scientific (Fairlawn, NJ). Copper(I) acetate, 4-azidobutanoic acid, *N*-methyl-2-pyrrolidone (NMP), trifluoroacetic acid (TFA), triisopropylsilane (TIS), triethylamine (TEA), diisopropylethylamine (DIEA), and deuterated DMSO were purchased from Sigma-Aldrich (St. Louis, MO).

Peptide Synthesis. A collagen-like peptide with the sequence (GPO)₈GG and four elastin-like peptides with sequence VPGFGV-PGFGVPGWGVPGFGG' (FFWF), VPGFGVPGWGVP-GWGVPGFGG' (FWWF), VPGWGVPGWGVPGWGVPGWGVPGFGG' (WWWF), and VPGWGVPGWGVPGWGVPGWGG' (WWWW) (G': propargylglycine) were synthesized via traditional solid-phase peptide synthesis methods (SPPS) using a Focus XC automatic peptide synthesizer (AAPPTec Inc., Louisville, KY) (Scheme S1). Rink amide polystyrene resin with a loading capacity of 0.19 mmol/g was used for the synthesis. HBTU was used to activate the amino acids for coupling in the presence of 2 M diisopropylethylamine (DIEA) in NMP. Deprotection of the Fmoc group was conducted using 20% piperidine in DMF. We used 45 min coupling cycles for all the residues. Double coupling with 4:1 amino acid/resin ratio was used for the conjugation. 4-Azidobutanoic acid was manually attached to the N-terminus of the (GPO)8GG on resin. The alkyne group from propargylglycine was introduced to each C-terminus of the ELP sequences. Cleavage of these peptides from the resin was conducted in 92:4.5:2.5 (v:v:v) trifluoroacetic acid (TFA)/triisopropylsilane (TIS)/water for 4 h. The TFA was mostly evaporated, and the cleaved peptide was precipitated in cold ether. The peptide was then redissolved in water and lyophilized. Crude peptides were purified via reverse-phase HPLC (Waters Inc., Milford, MA) on a Waters Xbridge BEH130 Prep C-18 column. The mobile phase comprised gradients of degassed deionized water with 0.1% TFA and acetonitrile with 0.1% TFA, at a flow rate of 21 mL/min. Peptide was detected by a UV detector at 214 nm; fractions with product were collected and lyophilized. The molecular weight of the peptides was confirmed via electrospray ionization mass spectrometry (ESI-MS, ACQUITY UPLC H-Class/SQD2, VG Analytical, Manchester, UK), and the

purity of the peptide was confirmed via analytical scale, reverse-phase HPLC (Waters 2996; symmetry C18, 3.5 μ m, 4.6 × 75 mm²).

ELP–CLP Conjugate Synthesis. These ELP–CLP conjugates were synthesized via the copper(I)-catalyzed alkyne—azide cycloaddition (CuAAC) "click" reaction (Scheme S1c). Equivalent CLP (7.14 mg, 3 μ mol) and ELP (3 μ mol) were dissolved in 1.0 mL of anhydrous dimethylformamide (DMF)/dimethyl sulfoxide (DMSO) (7:3). Then Cu(I) acetate (0.25 equiv to alkyne) was added to the solution. The mixture was stirred at 80 °C under nitrogen for 20 h. After reaction, the resulting hybrid copolymer was isolated into a 7-fold volume of cold diethyl ether and redissolved in water. The conjugate solution was then dialyzed against water for 7 days to remove the residual catalyst. A dialysis membrane with MWCO of 1K Da was used for the process.

Nuclear Magnetic Resonance Spectrometry (NMR). $^1{\rm H}$ NMR spectra were recorded under standard quantitative conditions on a Bruker AVIII spectrometer operating at 600 MHz, using 128 scans. All samples were dissolved in deuterated dimethyl sulfoxide (δ (d_6 -DMSO) = 2.50 ppm) at a concentration of 1 mg/mL. The resulting spectra were analyzed using Mnova software (Mestrelab Research, Santiago deCompostela, Spain).

Fourier Transform Infrared Spectroscopy (FTIR). FTIR spectra were collected using a Thermo Nicolet Nexus 670 (Thermo Scientific, Waltham, MA) spectrometer with a DuraSamplIR II ATR accessory (Smiths Detection, Danbury, CT). The peptide samples were added as solids onto the silicon ATR crystal and gently pressed down during data acquisition (128 scans at 4 cm⁻¹ resolution from 1000 to 4000 cm⁻¹).

Circular Dichroism Spectroscopy (CD). Cicular dichroic spectroscopy (Jasco 810 circular dichroism spectropolarimeter, Jasco Inc., Easton, MD) was conducted for the characterization of the secondary structure of the CLP domain. CLP and ELP–CLP conjugates were dissolved at a concentration of 100 μ M in PBS (10 mM, pH 7.4, 137 mM NaCl and 2.7 mM KCl) and incubated at 4 °C overnight before measurement. The CD spectra were recorded using quartz cells with a 0.2 cm optical path length. Full wavelength scans were collected to study the conformation of the peptide domain at 4 °C. The scanning rate was 50 nm/min, with a response time of 4 s. The wavelength scans were obtained from 200 to 250 nm and were recorded every 1 nm. To measure the melting temperature of the CLP domain, variable temperature experiments were conducted at maximum wavelength in each ELP–CLP conjugate (e.g., 225 nm) with a 10 °C/h heating rate from 4 to 80 °C.

Dynamic Light Scattering (DLS). Analysis of particle sizes in solution was conducted via DLS on a ZetaSizer Nano Series (Nano ZS, Malvern Instruments, UK) at a scattering angle of 173°, and data fitting was performed by using the cumulant method. All samples (1 mg) were dissolved in deionized water with the concentration of 1 mg/mL. ELP–CLP conjugates were incubated at 80 $^{\circ}\text{C}$ for 10 min and cooled at room temperature overnight before measurement. The lower critical solution temperature (LCST) of ELP-CLP conjugates was assessed by measurement of the average size of particles at temperatures from 5 to 80 °C, at an interval of 5 °C. These samples were uniformly cloudy with no evidence of settling during the time course of the DLS experiment. Samples were incubated at each temperature for 10 min before measurements. The LCST was assigned as the temperature at which the intensity of scattered light began to increase. The reported data represent an average of at least three measurements.

Transmission Electron Microscopy (TEM). Samples for TEM were prepared on carbon-coated copper grids (CF300-Cu, Electron Microscopy Sciences Inc.). The grids, pipet tips, and samples were incubated in an isothermal oven (VWR Signature Forced Air Safety Ovens, VWR Inc.) at desired temperature (4, 25, 37, 50, and 80 $^{\circ}$ C) for at least 1 h before sample preparation, which was also conducted in the oven. The ELP–CLP conjugate sample was dissolved in water at concentration of 1 mg/mL (consistent with DLS exeperiments and to prevent precipitation of the PTA stain). The samples were agitated prior to their addition to the grid. An aliquot (5 μ L) of the sample solution was drop cast on the grid and blotted after 60 s. For staining,



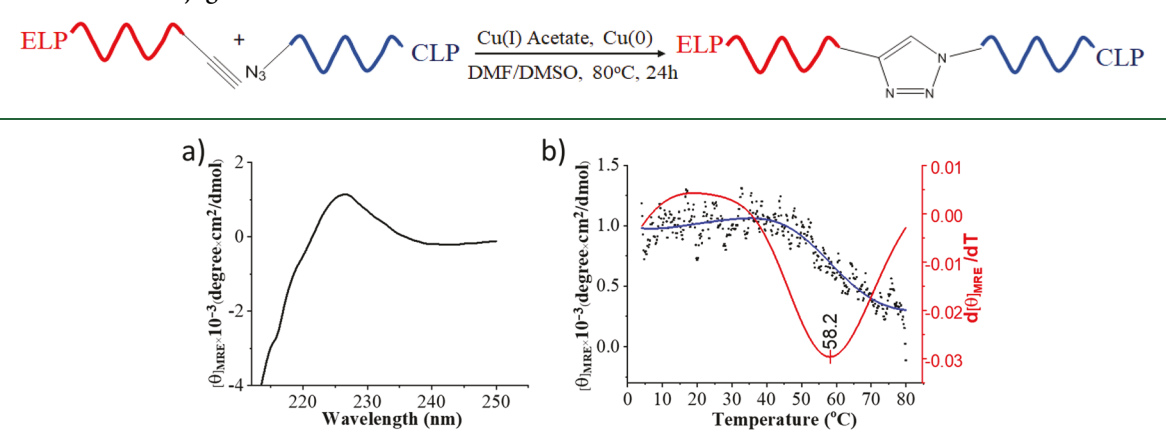


Figure 1. CD spectra showing a representative (a) full-wavelength scan and (b) thermal unfolding profile, here for the WWWW-(GPO)₈GG conjugate dissolved at a concentration of 100 μ M in PBS (pH 7.4). In (b), the first derivative of the unfolding curve with respect to temperature is shown in red.

2% phosphotungstic acid (PTA) (pH adjusted to 7.0 using 1 M NaOH) as a negative stain was used. A 3 μ L aliquot of the PTA solution was drop cast on the grid and blotted after 10 s. The sample was allowed to dry in the oven at the desired temperature for 1 h and then was air-dried for 2 h. TEM images were collected on a 2.1 TEM Tecnai 12 (JEOL USA Inc., Peabody, MA) at an acceleration voltage of 200 keV. Each ELP-CLP conjugate was produced and characterized three separate times with essentially identical behavior observed for the three separate synthetic replicates of each conjugate.

Ultraviolet–Visible Spectroscopy (UV–Vis). The $\pi-\pi$ interaction between the indole rings of the tryptophan residues in the ELP domain was assessed by UV–vis spectroscopy conducted on a Cary 60 UV–vis spectrophotometer (Agilent Technologies, Santa Clara, CA) at room temperature. At first, Rhodamine B (RB) was dissolved in DI water at a concentration of 0.1 mg/mL. Three different ELPs (FWWF, WWWF, and WWWW) were added into separate RB solutions at a concentration 20 times that of the RB. The pH of the four samples was each adjusted to 4.5 by addition of a small volume of HNO₃. The maximum absorption wavelength of each solution was monitored to determine the presence of $\pi-\pi$ interactions in the ELP solutions, as assessed by a change in the maximum relative to that of the RB solution, where λ_{max} is 554 nm.

Atomic Force Microscopy (AFM). The thickness of the platelets in each sample was determined by AFM measurements (Dimension 3100 V SPM, Bruker). ELP—CLP conjugates with a concentration of 0.5 mg/mL in DI water were prepared according to the protocol described above. The samples were agitated prior to their placement onto the substrates for AFM analysis. A 50 μ L solution of a given ELP—CLP conjugate was dropped on a glass surface. The sample then was dried in air at room temperature overnight. AFM tips (Bruker, 40 N/m, 320 kHz) equipped with a 117 μ m × 33 μ m rectangular silicon probe were employed to image the plate-like nanoparticles in the sample.

RESULTS AND DISCUSSION

In this report, we investigate the inverse transition behavior and morphology of a select set of ELP–CLP conjugates with variations in the hydrophobicity of a short, peptide-based ELP domain. In our previous studies, a $(VPGFG)_5$ –CLP bioconjugate was produced and exhibited a targeted $T_{\rm t}$ of ~37 °C, which was desirable because of our interest in producing thermally responsive and collagen-binding nanostructures. The $(VPGFG)_5$ –CLP bioconjugate, however, self-assembled into large and generally ill-defined aggregates (~1000 nm), which we postulated may have resulted from insufficient hydrophobicity of the $(VPGFG)_5$. In an effort to

promote robust hydrophobic collapse of the ELP while maintaining a T_t with relevance for drug delivery, ELPs comprising variants of (VPGXG)₄ with various substitutions of F (phenylalanine) and W (tryptophan) were produced. The (VPGXG)₄ variants include FFWF, FWWF, WWWF, and WWWW, where these amino acid designations indicate the amino acid in the X position of each VPGXG pentapeptide motif (e.g., FFWF represents VPGFG VPGFG VPGWG VPGFGG', where G' is propargylglycine). The WWWW sequence was expected to show the lowest T_t , based on the functional scale reported initially by Urry. 39,53 The CLP sequence (GPO)₈GG was employed due to the fact that CLPs with eight or more GPO repeats exhibit melting temperatures $(T_{\rm m})$ above 37 °C, 1,2,54 which enables formation of stable triple helix at physiological temperature and would be expected to support integration of the conjugates in/on collagencontaining matrices.

C-terminally alkyne-functionalized, short peptide-based ELPs and the N-terminally azide-functionalized CLP were synthesized via standard Fmoc-based solid-phase peptide synthesis methods (SPPS, Scheme S1) and purified via reverse-phase high-performance liquid chromatography (HPLC). The purity and expected composition of the peptides were verified by analytical HPLC and electrospray ionization mass spectrometry (ESI-MS), respectively (Figures S1 and S2). The ELPs were then conjugated to the CLP in dimethylformamide (DMF)/dimethyl sulfoxide (DMSO) via standard copper(I)-catalyzed alkyne-azide cycloaddition CuAAC methods (Scheme 1); successful synthesis and purification of the conjugates in high yield were verified via nuclear magnetic resonance spectrometry (¹H NMR) spectroscopy (Figures S3-S10) as well as Fourier transform infrared (FT-IR) spectroscopy (Figures S11-S14).

Circular dichroism (CD) spectroscopy was conducted to confirm triple-helix formation by the CLP domain in the ELP—CLP conjugates. Figure 1a presents the full-wavelength scan from 215 to 250 nm for the WWWW-b-(GPO)₈GG conjugate, which exhibits a clear maximum at 225 nm, indicating that the CLP domain is capable of forming a triple helix while conjugated to the most hydrophobic of the reported ELP domains. (CD spectra of the ELP-only peptides under the same conditions are featureless because of the short length of the ELP in our studies (not shown). The CD spectral data

from 190 to 210 nm were not reliable because of a very high dynode voltage (Figure S15) and are therefore not presented.) The reduction of the intensity of the peak at 225 nm with increasing temperature (Figure 1b, blue curve) demonstrated the unfolding of the triple helix upon heating. The first derivative of the melting curve (Figure 1b, red curve) indicated the melting temperature of the CLP is ~58.2 °C, which is elevated relative to that of the isolated CLP (~54.4 °C, Figure S16). Presumably, the collapse of the ELP domain at the elevated temperatures anchors the CLP and stabilizes it against unfolding, consistent with our previously reported results. 28,30,51 The other ELP-CLP conjugates showed similar $T_{\rm m}$ values (Figure S17), indicating that the increased stability of the CLP domain against unfolding was not significantly altered by variations in the composition of the ELP domain, as might be expected. Once the ELP domain collapses, it simply serves to generally anchor the CLP against unfolding, regardless of the amino acid composition of the ELP domain.

Dynamic light scattering (DLS) studies were conducted to investigate the assembly behavior of the ELP-CLP bioconjugates. The hydrodynamic diameter (D_h) of the assemblies was plotted as a function of temperature upon heating (Figure 2). The D_h of the FFWF-(GPO)₈GG

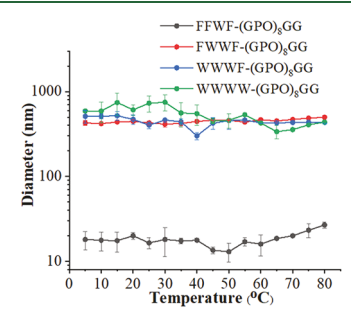


Figure 2. Hydrodynamic diameters of nanostructures as a function of temperature upon heating. All samples were dissolved in deionized water with concentration of 1 mg/mL (pH = 6.2).

conjugate remained below 20 nm for the entire temperature range of the experiment, suggesting a lack of assembly (which

was confirmed by TEM analysis (Figure S18); ELP monomers alone exhibit $D_{\rm h}$ of ~10 nm). In contrast, the other three ELP–CLP conjugates self-assembled into structures with an apparent $D_{\rm h}$ of ~500 nm, despite the fact that the FWWF and WWWF ELPs alone did not show any assembly over the full temperature range and the WWWW ELP because of its greater hydrophobicity, exhibited mainly spherical structures with $D_{\rm h}$ of only ~120 nm at temperatures >4 °C (Figure S19). These data are consistent with our previous report indicating that the assembly of the FWWF and WWWF conjugates is triggered by the reduction in $T_{\rm t}$ of the ELP domains after conjugation with CLP and that the morphology of the WWWW conjugates is altered as a result of conjugation (see below).

While it is well accepted that amino acid substitutions for X in the (VPGXG) domains of high-molecular-weight ELPs can substantially modify phase separation behavior, our results also illustrate the high sensitivity of the ELP-CLP conjugate assembly to the substitution of a single amino acid in the short, peptide-based ELP domain. The $T_{\rm t}$ of the FFWF-(GPO)₈GG conjugate was higher than 80 °C (and thus showed only low D_h values in the DLS experiments). One additional W substitution to the FFWF sequence (to yield FWWF) dramatically reduced the $T_{\rm t}$ of the conjugates to below 4 $^{\circ}$ C, likely a result of the lower transition temperatures of the more hydrophobic ELPs.³⁹ The structures, once formed, show high thermal stability, remaining intact at temperatures of at least 80 °C, even at temperatures at which the CLP domain is suggested, via CD studies (Figure 1), to unfold. This suggests that the FWWF, WWWF, and WWWW ELP domains are significantly stable against dissolution once collapsed.

Transmission electron microscopy (TEM) was conducted to investigate the morphology of the nanostructures self-assembled from the ELP–CLP diblock conjugates at 25, 37, 50, and 80 °C (Figure 3). As expected, the FFWF-(GPO)₈GG conjugate did not form any well-defined nanostructures at any of the temperatures studied, as the $T_{\rm t}$ of the FFWF conjugate is higher than 80 °C (Figure 2 and Figure S19). However, the other conjugates (FWWF, FWWW, and WWWW) all formed nanoparticles which surprisingly, when compared with the vesicle-forming (VPGFG)₆-(GPO)₄GFOGER(GPO)₄GG of

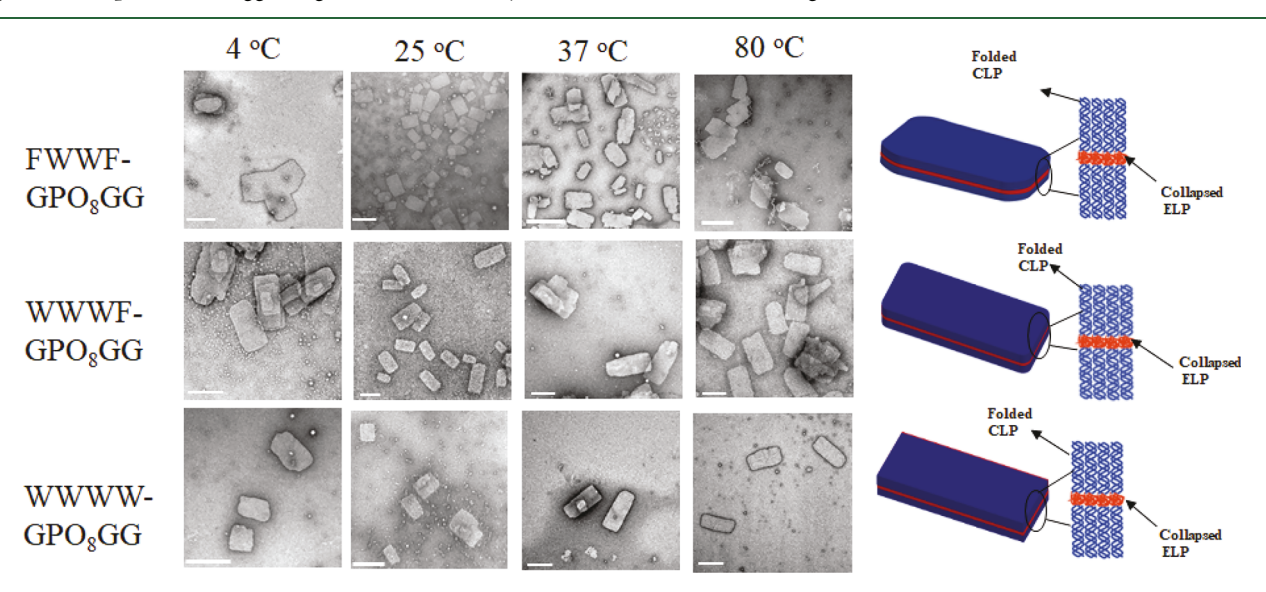


Figure 3. TEM images of nanostructures self-assembled from water solutions of ELP-CLP bioconjugates at various temperatures, after negative staining with 2% phosphotungstic acid. Scale bars: 500 nm.

Biomacromolecules

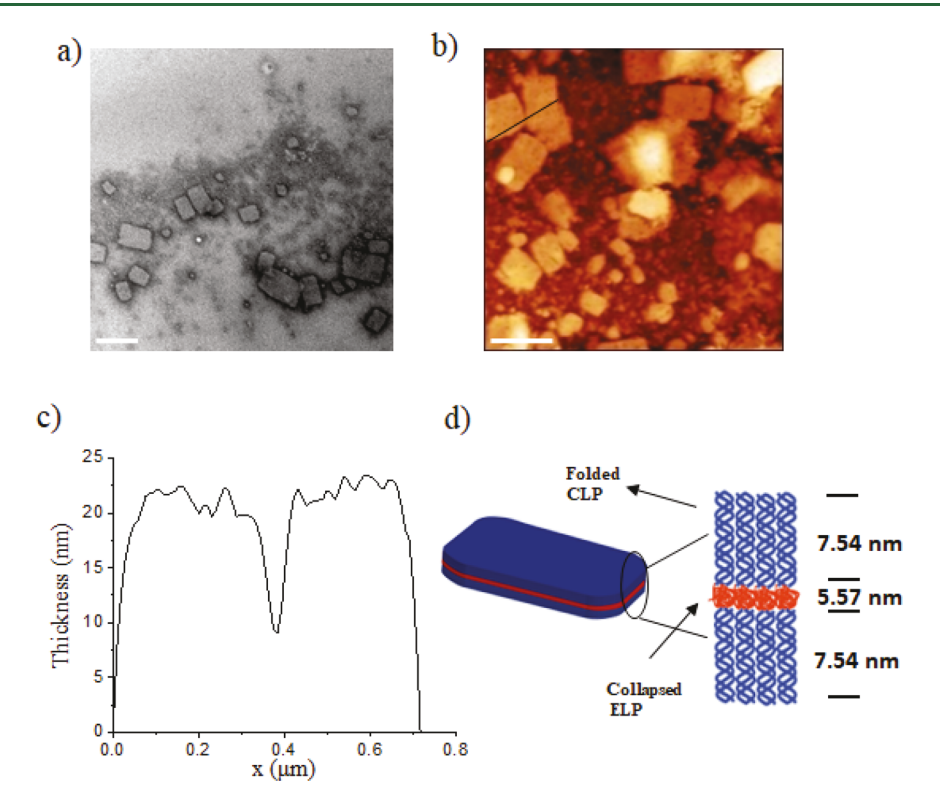


Figure 4. Microscopy measurements of the FWWF-(GPO)₈GG conjugates: (a) TEM image of assemblies at room temperature; (b) AFM image of assemblies at room temperature; (c) the thickness curve of the plate-like nanoparticles (along the black line in (b)); (d) proposed structure of the assemblies. Scale bars: 500 nm.

our previous work, 51 exhibited nonspherical, plate-like structures. The dimensions of the platelets are quite uniform $(200 \pm 20 \text{ nm} \times 500 \pm 20 \text{ nm} \text{ for all three conjugates})$ and consistent with the DLS results (Figure 2). Furthermore, these plate-like nanostructures remained perfectly intact at elevated temperatures, even above the CLP melting temperature, likely because of the strong interaction between the indole rings of the tryptophan residues in the ELP domain (shown in Figure ⁻⁵⁷ Potential organization of the ELP–CLP conjugates is shown in Figure 3; selected area electron diffraction (SAED) data of the ELP-CLP peptide (WWWF-(GPO)₈GG) indicated that the platelets are not crystalline (Figure S23). Slight differences in the orthogonality of the corners of the platelets (the WWWW-containing conjugates show nearly uniform right angles for corners, while the other conjugates show more rounded corners) indicate that the assembly is very sensitive to the composition of the ELP domain. The polydispersity of the platelets (observed here and also shown in the DLS data in Figure S24) likely results from the presence of some unassembled material as well as platelets that may be aggregated. It is possible that the self-assembly of these rectangular platelets (rather than vesicles) is driven by increased stability of the ELP layer because of the $\pi-\pi$ stacking of the tryptophan indole side chains, consistent with the reports of Stenzel and Thordarson, in which a diblock terpolymer PEG-b-P(NIPAM-co-PDMI) self-assembled into nonspherical polymersome morphologies at various concentrations and solvent compositions, owing to the $\pi-\pi$ interactions of the perylene aromatic side chains. 58-60 Hamley and co-workers have also demonstrated the enhancement of assembly promoted by phenylalanine residues in model peptides based on the KLVFF motif.⁶¹

The plate-like structure and thickness were further investigated via atomic force microscopy (AFM, Figure 4). Both TEM and AFM figures confirm the plate-like structure of FWWF-b-(GPO)₈GG conjugates with dimensions of approximately 200 nm × 500 nm. Analysis of the AFM images indicates that the thickness of the plates was 20.6 ± 0.3 nm for the FWWF-(GPO)₈GG conjugate (Figure 4b,c and Figure \$20), which is perfectly consistent with those observed for the WWWF- and WWWW-containing conjugates (Figure S25) and with the calculated length of two CLP triple helices and the thickness of the collapsed ELP domain (Figure S26), thus further corroborating the proposed structure (Figure 4d and Figure S26). To further assess the possible crystallinity of the platelets, SAXS experiments of individual samples were conducted to complement the SAED evaluated in the TEM analysis. The SAXS data (Figure S23) showed a peak characteristic of the collagen triple helix but did not exhibit any other features, suggesting that the ELP region of the bilayer does not exhibit crystalline ordering.

There have been very limited reports of thermoresponsive nanostructures that can be assembled from short synthetic ELPs (in contrast to the myriad studies of long recombinant ELPs), with previous studies largely focused on the modification of polymers and dendrimers. 46-49,62-64 Our previous work illustrated that the simple anchoring of three short ELP peptides to a collagen triple helix is sufficient to induce an LCST-like transition that can drive self-assembly, and our current studies illustrate that with judicious choice of ELP sequence the phenomenon is applicable to conjugates with ELP domains containing as few as four (VPGXG) repeats. Our initial interest in these conjugates derived from their potential to exhibit thermally responsive assembly for targeted delivery applications. While the conjugates reported here lack

this thermal responsiveness (forming nanoparticles at all temperatures studied), our current work highlights the interesting possibility that increasing the aromaticity of the ELP domains may afford additional opportunities for the formation of peptide-based nanosheets and nanoplates. Collagen-localized delivery of drugs from loaded ELP—CLP platelets is still likely to be possible, although such delivery would not be thermally triggered. Our previous studies suggest the possibility of delayed release of hydrophobic compounds from collagen films by virtue of the sequestration of loaded ELP—CLP conjugates via triple-helix formation, and it is reasonable to expect that such delivery may be possible from the conjugates reported here.

Indeed, preliminary studies of (GPO)₈ conjugates produced with ELP domains in which substitutions of W with Y were made have demonstrated that the Y-containing conjugates can also adopt plate-like morphologies with similar dimensions (Figure S27a,b). This observed behavior does not appear to be driven strictly by the inclusion of W in the ELP domain, as FWWF-b-(GPO)₇GG conjugates fail to form nanoscale plates and instead adopt a spherical morphology (Figure S27c). Complementary computational and experimental studies are underway to determine additional compositional, sequence, and processing details that underpin the formation of various nanostructures from this class of peptide sequences and will be reported in due course.

CONCLUSIONS

We report the assembly behavior of a set of (VPGXG)₄-(GPO)₈ bioconjugates and demonstrate that exceeding a threshold number of W residues results in the adoption of nanoscale platelet morphologies from these molecules, in contrast to our previous reports of vesicular assemblies. Increased stability of the collapsed W-containing conjugates may arise from the increased hydrophobicity (according to the scale reported by Urry) and/or increased π – π stacking in these domains, afforded by the W residue. While the increased stability of the ELPs of high aromatic character precludes any thermally responsive behavior from these bioconjugates under standard aqueous experimental conditions, the aromatic character of the bilayer interior of these nanoparticles, regardless of their shape, may afford useful advantages for the encapsulation of hydrophobic (and/or aromatic) drugs such as doxorubicin, dexamethasone, and paclitaxel.⁶⁷ Additionally, the collagen domains at the surface of the nanoplates, as we have demonstrated for vesicular nanoparticles, may serve as a means to localize these nanoplates in or on collagen-containing substrates. 25,68,69 Additional computational and experimental studies are underway to devise more detailed rules to guide the design and assembly of this class of bioconjugates.

ASSOCIATED CONTENT

S Supporting Information

The Supporting Information is available free of charge on the ACS Publications website at DOI: 10.1021/acs.bio-mac.8b01681.

Experimental section; peptide and conjugate synthesis; characterization of conjugates (NMR, MS, FTIR, CD, DLS, TEM, AFM); supplemental CD, DLS, SAXS data (PDF)

AUTHOR INFORMATION

Corresponding Author

*E-mail kiick@udel.edu.

ORCID ®

Kristi L. Kiick: 0000-0001-8587-0301

Author Contributions

J.Q. and T.L. contributed equally to this work.

Notes

The authors declare no competing financial interest.

ACKNOWLEDGMENTS

This work was funded in part by the National Institutes of Health (R21 AR069778A, 1 P30 GM110758, and both 1 P30 GM103519 and 1 P20 104316 for instrument resources) and in part by the National Science Foundation (CBET 1703402). We thank Chaoying Ni, Jen Sloppy, Yong Zhao, and Darrin Pochan at the University of Delaware for advice and assistance with TEM.

REFERENCES

- (1) Luo, T. Z.; Kiick, K. L. Collagen-like peptides and peptide-polymer conjugates in the design of assembled materials. *Eur. Polym. J.* **2013**, *49* (10), 2998–3009.
- (2) Yu, S. M.; Li, Y.; Kim, D. Collagen mimetic peptides: progress towards functional applications. *Soft Matter* **2011**, *7* (18), 7927–7938.
- (3) Shoulders, M. D.; Raines, R. T. Collagen Structure and Stability. *Annu. Rev. Biochem.* **2009**, *78*, 929–958.
- (4) Fallas, J. A.; Dong, J. H.; Tao, Y. Z. J.; Hartgerink, J. D. Structural Insights into Charge Pair Interactions in Triple Helical Collagen-like Proteins. *J. Biol. Chem.* **2012**, *287* (11), 8039–8047.
- (5) Persikov, A. V.; Ramshaw, J. A. M.; Brodsky, B. Prediction of collagen stability from amino acid sequence. *J. Biol. Chem.* **2005**, 280 (19), 19343–19349.
- (6) He, L. R.; Theato, P. Collagen and collagen mimetic peptide conjugates in polymer science. *Eur. Polym. J.* **2013**, 49 (10), 2986–2997.
- (7) Strauss, K.; Chmielewski, J. Advances in the design and higherorder assembly of collagen mimetic peptides for regenerative medicine. *Curr. Opin. Biotechnol.* **2017**, *46*, 34–41.
- (8) Acevedo-Jake, A. M.; Ngo, D. H.; Hartgerink, J. D. Control of Collagen Triple Helix Stability by Phosphorylation. *Biomacromolecules* **2017**, *18* (4), 1157–1161.
- (9) Jiang, T.; Meyer, T. A.; Modlin, C.; Zuo, X.; Conticello, V. P.; Ke, Y. Structurally Ordered Nanowire Formation from Co-Assembly of DNA Origami and Collagen-Mimetic Peptides. *J. Am. Chem. Soc.* **2017**, *139* (40), 14025–14028.
- (10) O'Leary, L. E. R.; Fallas, J. A.; Bakota, E. L.; Kang, M. K.; Hartgerink, J. D. Multi-hierarchical self-assembly of a collagen mimetic peptide from triple helix to nanofibre and hydrogel. *Nat. Chem.* **2011**, 3 (10), 821–828.
- (11) Rele, S.; Song, Y. H.; Apkarian, R. P.; Qu, Z.; Conticello, V. P.; Chaikof, E. L. D-periodic collagen-mimetic microfibers. *J. Am. Chem. Soc.* **2007**, *129* (47), 14780–14787.
- (12) Krishna, O. D.; Kiick, K. L. Supramolecular Assembly of Electrostatically Stabilized, Hydroxyproline-Lacking Collagen-Mimetic Peptides. *Biomacromolecules* **2009**, *10* (9), 2626–2631.
- (13) Tanrikulu, I. C.; Forticaux, A.; Jin, S.; Raines, R. T. Peptide tessellation yields micrometre-scale collagen triple helices. *Nat. Chem.* **2016**, *8*, 1008.
- (14) Wang, A. Y.; Mo, X.; Chen, C. S.; Yu, S. M. Facile modification of collagen directed by collagen mimetic peptides. *J. Am. Chem. Soc.* **2005**, *127* (12), 4130–4131.
- (15) Li, Y.; Foss, C. A.; Summerfield, D. D.; Doyle, J. J.; Torok, C. M.; Dietz, H. C.; Pomper, M. G.; Yu, S. M. Targeting collagen strands by photo-triggered triple-helix hybridization. *Proc. Natl. Acad. Sci. U. S. A.* **2012**, *109* (37), 14767–14772.

Biomacromolecules

(16) Zitnay, J. L.; Li, Y.; Qin, Z.; San, B. H.; Depalle, B.; Reese, S. P.; Buehler, M. J.; Yu, S. M.; Weiss, J. A. Molecular level detection and localization of mechanical damage in collagen enabled by collagen hybridizing peptides. *Nat. Commun.* **2017**, *8*, 14913.

- (17) Wahyudi, H.; Reynolds, A. A.; Li, Y.; Owen, S. C.; Yu, S. M. Targeting collagen for diagnostic imaging and therapeutic delivery. *J. Controlled Release* **2016**, 240, 323–331.
- (18) San, B. H.; Li, Y.; Tarbet, E. B.; Yu, S. M. Nanoparticle Assembly and Gelatin Binding Mediated by Triple Helical Collagen Mimetic Peptide. ACS Appl. Mater. Interfaces 2016, 8 (31), 19907–19015
- (19) San, B. H.; Hwang, J. M.; Sampath, S.; Li, Y.; Bennink, L. L.; Yu, S. M. Self-Assembled Water-Soluble Nanofibers Displaying Collagen Hybridizing Peptides. *J. Am. Chem. Soc.* **2017**, *139* (46), 16640–16649.
- (20) Hwang, J. M.; San, B. H.; Turner, N. J.; White, L. J.; Faulk, D. M.; Badylak, S. F.; Li, Y.; Yu, S. M. Molecular assessment of collagen denaturation in decellularized tissues using a collagen hybridizing peptide. *Acta Biomater.* **2017**, *53*, 268–278.
- (21) Hwang, J.; Huang, Y. F.; Burwell, T. J.; Peterson, N. C.; Connor, J.; Weiss, S. J.; Yu, S. M.; Li, Y. In Situ Imaging of Tissue Remodeling with Collagen Hybridizing Peptides. *ACS Nano* **2017**, *11* (10), 9825–9835.
- (22) Converse, M. I.; Walther, R. G.; Ingram, J. T.; Li, Y.; Yu, S. M.; Monson, K. L. Detection and characterization of molecular-level collagen damage in overstretched cerebral arteries. *Acta Biomater.* **2018**, *67*, 307–318.
- (23) Bennink, L. L.; Smith, D. J.; Foss, C. A.; Pomper, M. G.; Li, Y.; Yu, S. M. High Serum Stability of Collagen Hybridizing Peptides and Their Fluorophore Conjugates. *Mol. Pharmaceutics* **2017**, *14* (6), 1906–1915.
- (24) Urello, M. A.; Kiick, K. L.; Sullivan, M. O. ECM turnover-stimulated gene delivery through collagen-mimetic peptide-plasmid integration in collagen. *Acta Biomater.* **2017**, *62*, 167–178.
- (25) Urello, M. A.; Kiick, K. L.; Sullivan, M. O. A CMP-based method for tunable, cell-mediated gene delivery from collagen scaffolds. *J. Mater. Chem. B* **2014**, 2 (46), 8174–8185.
- (26) Luo, T. Z.; David, M. A.; Dunshee, L. C.; Scott, R. A.; Urello, M. A.; Price, C.; Kiick, K. L. Thermoresponsive Elastin-b-Collagen-Like Peptide Bioconjugate Nanovesicles for Targeted Drug Delivery to Collagen-Containing Matrices. *Biomacromolecules* **2017**, *18* (8), 2539–2551.
- (27) Luo, J. N.; Tong, Y. W. Self-Assembly of Collagen-Mimetic Peptide Amphiphiles into Biofunctional Nanofiber. *ACS Nano* **2011**, 5 (10), 7739–7747.
- (28) Krishna, O. D.; Wiss, K. T.; Luo, T. Z.; Pochan, D. J.; Theato, P.; Kiick, K. L. Morphological transformations in a dually thermoresponsive coil-rod-coil bioconjugate. *Soft Matter* **2012**, *8* (14), 3832–3840.
- (29) Luo, T. Z.; Kiick, K. L. Collagen-like peptide bioconjugates. *Bioconjugate Chem.* **2017**, 28 (3), 816–827.
- (30) Luo, T. Z.; He, L. R.; Theato, P.; Kiick, K. L. Thermoresponsive Self-Assembly of Nanostructures from a Collagen-Like Peptide-Containing Diblock Copolymer. *Macromol. Biosci.* **2015**, *15* (1), 111–123.
- (31) Foster, J. A.; Bruenger, E.; Gray, W. R.; Sandberg, L. B. Isolation and Amino-Acid Sequences of Tropoelastin Peptides. *J. Biol. Chem.* **1973**, 248 (8), 2876–2879.
- (32) Urry, D. W. Physical chemistry of biological free energy transduction as demonstrated by elastic protein-based polymers. *J. Phys. Chem. B* **1997**, *101* (51), 11007–11028.
- (33) Kojima, C.; Irie, K. Synthesis of temperature-dependent elastin-like peptide-modified dendrimer for drug delivery. *Biopolymers* **2013**, *100* (6), 714–21.
- (34) Massodi, I.; Bidwell, G. L.; Raucher, D. Evaluation of cell penetrating peptides fused to elastin-like polypeptide for drug delivery. *J. Controlled Release* **2005**, *108* (2–3), 396–408.
- (35) Weitzhandler, I.; Dzuricky, M.; Hoffmann, I.; Quiroz, F. G.; Gradzielski, M.; Chilkoti, A. Micellar Self-Assembly of Recombinant

Resilin-/Elastin-Like Block Copolypeptides. *Biomacromolecules* **2017**, 18 (8), 2419-2426.

- (36) Pille, J.; van Lith, S. A. M.; van Hest, J. C. M.; Leenders, W. P. J. Self-Assembling VHH-Elastin-Like Peptides for Photodynamic Nanomedicine. *Biomacromolecules* **2017**, *18* (4), 1302–1310.
- (37) Nawroth, J. F.; McDaniel, J. R.; Chilkoti, A.; Jordan, R.; Luxenhofer, R. Maleimide-Functionalized Poly(2-Oxazoline)s and Their Conjugation to Elastin-Like Polypeptides. *Macromol. Biosci.* **2016**, *16* (3), 322–333.
- (38) McDaniel, J. R.; Radford, D. C.; Chilkoti, A. A Unified Model for De Novo Design of Elastin-like Polypeptides with Tunable Inverse Transition Temperatures. *Biomacromolecules* **2013**, *14* (8), 2866–2872.
- (39) Nuhn, H.; Klok, H. A. Secondary Structure Formation and LCST Behavior of Short Elastin-Like Peptides. *Biomacromolecules* **2008**, 9 (10), 2755–2763.
- (40) Martin, L.; Castro, E.; Ribeiro, A.; Alonso, M.; Rodriguez-Cabello, J. C. Temperature-Triggered Self-Assembly of Elastin-Like Block Co-Recombinamers: The Controlled Formation of Micelles and Vesicles in an Aqueous Medium. *Biomacromolecules* **2012**, *13* (2), 293–298.
- (41) Park, W. M.; Champion, J. A. Thermally Triggered Self-Assembly of Folded Proteins into Vesicles. *J. Am. Chem. Soc.* **2014**, 136 (52), 17906–17909.
- (42) Garcia-Arevalo, C.; Bermejo-Martin, J. F.; Rico, L.; Iglesias, V.; Martin, L.; Rodriguez-Cabello, J. C.; Arias, F. J. Immunomodulatory Nanoparticles from Elastin-Like Recombinamers: Single-Molecules for Tuberculosis Vaccine Development. *Mol. Pharmaceutics* **2013**, *10* (2), 586–597.
- (43) Fujita, Y.; Mie, M.; Kobatake, E. Construction of nanoscale protein particle using temperature-sensitive elastin-like peptide and polyaspartic acid chain. *Biomaterials* **2009**, *30* (20), 3450–3457.
- (44) Shi, P.; Gustafson, J. A.; MacKay, J. A. Genetically engineered nanocarriers for drug delivery. *Int. J. Nanomed.* **2014**, *9*, 1617–1626.
- (45) Fernandez-Trillo, F.; Dureault, A.; Bayley, J. P. M.; van Hest, J. C. M.; Thies, J. C.; Michon, T.; Weberskirch, R.; Cameron, N. R. Elastin-based side-chain polymers: Improved synthesis via RAFT and stimulus responsive behavior. *Macromolecules* **2007**, *40* (17), 6094–6099.
- (46) Kojima, C.; Irie, K.; Tada, T.; Tanaka, N. Temperature-Sensitive Elastin-Mimetic Dendrimers: Effect of Peptide Length and Dendrimer Generation to Temperature Sensitivity. *Biopolymers* **2014**, *101* (6), 603–612.
- (47) Kojima, C.; Irie, K. Synthesis of Temperature-Dependent Elastin-Like Peptide-Modified Dendrimer for Drug Delivery. *Biopolymers* **2013**, *100* (6), 714–721.
- (48) Kojima, C.; Fukushima, D. Applications of Gold Nanoparticle-Loaded Thermosensitive Elastin-Mimetic Dendrimer to Photothermal Therapy. *J. Photopolym. Sci. Technol.* **2016**, 29 (4), 519–523.
- (49) Fukushima, D.; Sk, U. H.; Sakamoto, Y.; Nakase, I.; Kojima, C. Dual stimuli-sensitive dendrimers: Photothermogenic gold nanoparticle-loaded thermo-responsive elastin-mimetic dendrimers. *Colloids Surf., B* **2015**, *132*, 155–160.
- (50) Hassan, M.; Martin, A. D.; Thordarson, P. Engineering Biocompatible Scaffolds through the Design of Elastin-Based Short Peptides. *ChemPlusChem.* **2018**, 83 (1), 47–52.
- (51) Luo, T. Z.; Kiick, K. L. Noncovalent Modulation of the Inverse Temperature Transition and Self-Assembly of Elastin-b-Collagen-like Peptide Bioconjugates. *J. Am. Chem. Soc.* **2015**, *137* (49), 15362–15365.
- (52) Moreno-Villoslada, I.; Jofré, M.; Miranda, V.; González, R.; Sotelo, T.; Hess, S.; Rivas, B. L. pH Dependence of the Interaction between Rhodamine B and the Water-Soluble Poly(sodium 4-styrenesulfonate). *J. Phys. Chem. B* **2006**, *110* (24), 11809–11812.
- (53) Urry, D. W.; Luan, C. H.; Parker, T. M.; Gowda, D. C.; Prasad, K. U.; Reid, M. C.; Safavy, A. Temperature of polypeptide inverse temperature transition depends on mean residue hydrophobicity. *J. Am. Chem. Soc.* **1991**, *113* (11), 4346–4348.

Biomacromolecules

(54) Brodsky, B.; Persikov, A. V. Molecular structure of the collagen triple helix. In *Fibrous Proteins: Coiled-Coils, Collagen and Elastomers*; Parry, D.A.D., Squire, J. M., Eds.; Academic Press: San Diego, CA, 2005; p 301.

- (55) Xie, Y. Y.; Wang, X. C.; Huang, R. L.; Qi, W.; Wang, Y. F.; Su, R. X.; He, Z. M. Electrostatic and Aromatic Interaction-Directed Supramolecular Self-Assembly of a Designed Fmoc-Tripeptide into Helical Nanoribbons. *Langmuir* **2015**, 31 (9), 2885–2894.
- (56) Singh, P.; Brar, S. K.; Bajaj, M.; Narang, N.; Mithu, V. S.; Katare, O. P.; Wangoo, N.; Sharma, R. K. Self-assembly of aromatic alpha-amino acids into amyloid inspired nano/micro scaled architects. *Mater. Sci. Eng., C* **2017**, *72*, 590–600.
- (57) Podder, D.; Sasmal, S.; Maji, K.; Haldar, D. Supramolecular tryptophan-zipper forms a tripeptide as a regular proton transporter. *CrystEngComm* **2016**, *18* (22), 4109–4114.
- (58) Wong, C. K.; Mason, A. F.; Stenzel, M. H.; Thordarson, P. Formation of non-spherical polymersomes driven by hydrophobic directional aromatic perylene interactions. *Nat. Commun.* **2017**, 8 (1), 1240
- (59) Martinez, C. R.; Iverson, B. L. Rethinking the term "pistacking". Chem. Sci. 2012, 3 (7), 2191–2201.
- (60) Salonen, L. M.; Ellermann, M.; Diederich, F. Aromatic Rings in Chemical and Biological Recognition: Energetics and Structures. *Angew. Chem., Int. Ed.* **2011**, *50* (21), 4808–4842.
- (61) Castelletto, V.; Hamley, I. W.; Cenker, C.; Olsson, U.; Adamcik, J.; Mezzenga, R.; Miravet, J. F.; Escuder, B.; Rodriguez-Llansola, F. Influence of End-Capping on the Self-Assembly of Model Amyloid Peptide Fragments. *J. Phys. Chem. B* **2011**, *115* (9), 2107—2116.
- (62) Pechar, M.; Brus, J.; Kostka, L.; Konak, C.; Urbanova, M.; Slouf, M. Thermoresponsive self-assembly of short elastin-like polypentapeptides and their poly(ethylene glycol) derivatives. *Macromol. Biosci.* **2007**, *7* (1), 56–69.
- (63) van Eldijk, M. B.; Wang, J. C. Y.; Minten, I. J.; Li, C. L.; Zlotnick, A.; Nolte, R. J. M.; Cornelissen, J.; van Hest, J. C. M. Designing Two Self-Assembly Mechanisms into One Viral Capsid Protein. J. Am. Chem. Soc. 2012, 134 (45), 18506–18509.
- (64) Dai, M.; Haghpanah, J.; Singh, N.; Roth, E. W.; Liang, A.; Tu, R. S.; Montclare, J. K. Artificial Protein Block Polymer Libraries Bearing Two SADs: Effects of Elastin Domain Repeats. *Biomacromolecules* **2011**, *12* (12), 4240–4246.
- (65) Hamley, I. W.; Hutchinson, J.; Kirkham, S.; Castelletto, V.; Kaur, A.; Reza, M.; Ruokolainen, J. Nanosheet Formation by an Anionic Surfactant-like Peptide and Modulation of Self-Assembly through Ionic Complexation. *Langmuir* **2016**, 32 (40), 10387–10393.
- (66) Huang, H. Z.; Ganguly, D.; Chen, J. H.; Sun, X. Z. S. Conformational Flexibility and pH Effects on Anisotropic Growth of Sheet-Like Assembly of Amphiphilic Peptides. *J. Nanosci. Nanotechnol.* **2015**, *15* (6), 4470–4479.
- (67) Grecomoro, G.; Piccione, F.; Letizia, G. Therapeutic synergism between hyaluronic acid and dexamethasone in the intra-articular treatment of osteoarthritis of the knee: a preliminary open study. *Curr. Med. Res. Opin.* **1992**, *13* (1), 49–55.
- (68) Mo, X.; An, Y. J.; Yun, C. S.; Yu, S. M. Nanoparticle-assisted visualization of binding interactions between collagen mimetic peptide and collagen fibers. *Angew. Chem., Int. Ed.* **2006**, 45 (14), 2267–2270.
- (69) Li, Y.; Foss, C. A.; Summerfield, D. D.; Doyle, J. J.; Torok, C. M.; Dietz, H. C.; Pomper, M. G.; Yu, S. M. Targeting collagen strands by photo-triggered triple-helix hybridization. *Proc. Natl. Acad. Sci. U. S. A.* 2012, 109 (37), 14767–14772.